Journal of Materials Chemistry

www.rsc.org/materials

Volume 17 | Number 31 | 21 August 2007 | Pages 3273–3364

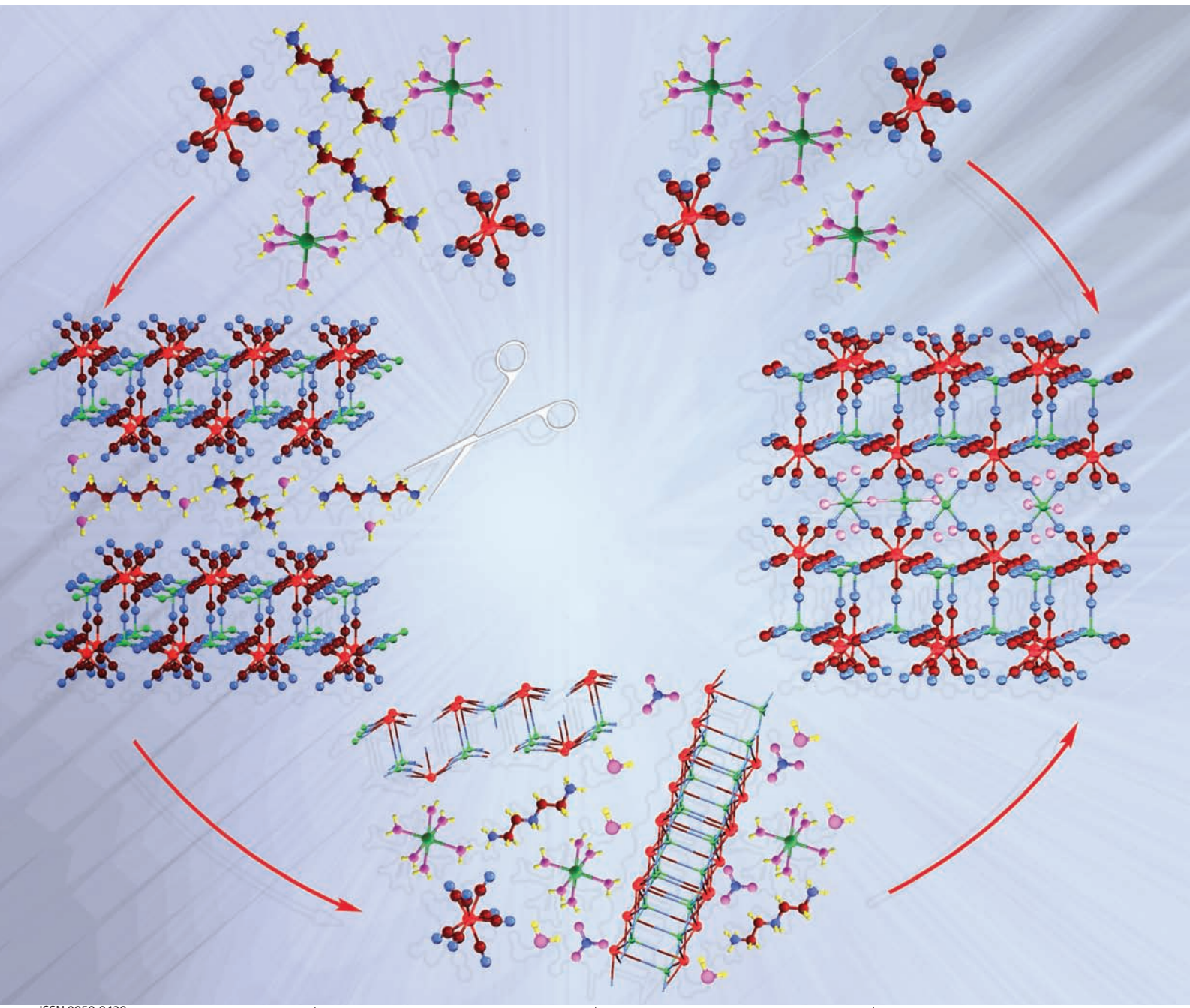

ISSN 0959-9428

RSC Publishing

0959-9428(2007)17:31;1-#

Exploring the formation of 3D ferromagnetic cyano-bridged $Cu^{II}_{2+x}\{Cu^{II}_4[W^V(CN)_8]_{4-2x}[W^{IV}(CN)_8]_{2x}\}\cdot yH_2O$ networks†

Robert Podgajny,*[a] Nikola Paul Chmel,[a] Maria Bałanda,[b] Piotr Tracz,[b] Bartłomiej Gaweł,[a] Dariusz Zając,[b] Marcin Sikora,[c] Czesław Kapusta,[c] Wiesław Łasocha,[a] Tadeusz Wasiutyński[b] and Barbara Sieklucka[a]

Received 12th March 2007, Accepted 4th May 2007
First published as an Advance Article on the web 16th May 2007
DOI: 10.1039/b703640j

Two novel non-stoichiometric 3D cyano-bridged coordination networks of general formula $Cu^{II}_{2+x}\{Cu^{II}_4[W^V(CN)_8]_{4-2x}[W^{IV}(CN)_8]_{2x}\}\cdot yH_2O$ were obtained according to two different synthetic strategies. The heterogeneous reaction between solid 2D cyano-bridged network $(dienH_3)\{Cu^{II}[W^V(CN)_8]\}_3\cdot 4H_2O$ (**1**) ($dienH_3^{3+}$ = protonated diethylenetriamine) and an aqueous solution of $Dy^{III}(NO_3)_3$ results in the removal of $dienH_3^{3+}$ cations and the formation of a 3D cyano-bridged $Cu^{II}_{2.44}\{Cu^{II}_4[W^V(CN)_8]_{3.12}[W^{IV}(CN)_8]_{0.88}\}\cdot 5H_2O$ (**2**) network. The direct combination of $[Cu^{II}(H_2O)_6]^{2+}$ and $[W^V(CN)_8]^{3-}$ in aqueous media leads to the structurally related $Cu^{II}_{2.97}\{Cu^{II}_4[W^V(CN)_8]_{2.06}[W^{IV}(CN)_8]_{1.94}\}\cdot 4H_2O$ (**3**) assembly. The assemblies **2** and **3** were characterised by X-ray powder diffraction along with IR, X-ray absorption spectroscopy (XAS), proton induced X-ray emission (PIXE) and magnetic measurements. **2** and **3** crystallise in a tetragonal system, space group *I*4/*mmm* with cell parameters $a = b = 7.2695(9)$ Å; $c = 28.268(5)$ Å; $Z = 2$ (**2**) and $a = b = 7.2858(9)$ Å, $c = 28.282(5)$ Å, $Z = 2$ (**3**). Both networks are characterised by the increase of T_C from 33 K to 40 K and coercivity from 0.2 to 2–2.5 kOe compared to **1**. Despite their general structural and magnetic similarity, **2** and **3** reveal significant differences in magnetic dimensionality: compound **2** exhibits the features of a metamagnet with a threshold field of 1.8 kOe at 4.2 K, while compound **3** resembles a classical magnet with 3D ordering. This difference is discussed in terms of non-stoichiometry of the networks accompanied by the appearance of different numbers of non-magnetic "defects" due to the formation of diamagnetic W(IV) centres.

Introduction

The strong interest in the design and construction of magnetic molecular materials has drawn much attention to 2D and 3D cyano-bridged copper-octacyanometalate (M = Mo, W) coordination networks.[1–20] The effective coupling along the M^V–CN–Cu^{II} linkage resulted in systems exhibiting long range magnetic ordering including examples of low temperature metamagnets.[1–5] The optical metal-to-metal charge transfer (MMCT) from $[Mo^{IV}(CN)_8]^{4-}$ to Cu^{II} moieties offered an opportunity to construct photomagnetic high-spin molecules as well as 3D systems characterised by reversible photo-switching between $\{Cu^{II}Mo^{IV}Cu^{II}\}$ and $\{Cu^{I}Mo^{V}Cu^{II}\}$ magnetic states.[1,6–9]

The diversity of cyano-bridged $Cu^{II}M^{V/IV}$ coordination architectures is an outcome of the variety of synthetic strategies employed. Several building block approaches were applied, including the direct combination of molecular precursors,[1,4,6,7,10–16,19] the use of assisting organic or inorganic molecules as blocking ligands,[2,17] bridging spacers[10,18] or counterions[3,9,10,17] along with the electrochemical synthesis[9] of a 3D $Cs_2Cu^{II}_7[Mo^{IV}(CN)_8]_4\cdot 6H_2O$ network with the use of a standard three-electrode set-up. Some examples of synthetic procedures highlight the unquestionable role of dynamic or/and static control of the competitive reactions (*i.e.* coordination equilibrium, precipitate formation, electrostatic equilibrium) in tuneable crystal growth process.[17]

Recently, we have synthesised and characterised a family of 2D coordination networks of the general formula $\{(LH_x)Cu^{II}_x[M^V(CN)_8]_x\cdot yH_2O\}_n$ (L = tetren (tetraethylenepentaamine), $x = 5$, $y = 9$; dien (diethylenetriamine), $x = 3$, $y = 4$; M = Mo, W).[20] The self-assembly process results in bilayered cyano-bridged $\{Cu^{II}[W^V(CN)_8]^-\}_n$ square grid backbones with interlayered protonated polyamine countercations and H_2O molecules. These compounds are characterised by long range ferromagnetic ordering with sharp phase transitions at T_C in range 28–37 K and coercivity in the range 30–225 Oe at $T = 4.3$ K. The interlayer distances between nitrogen atoms of terminal CN^- ligands of about 5.2–5.5 Å (Scheme 1) offer an opportunity to incorporate a third paramagnetic 3d or 4f

[a]*Faculty of Chemistry, Jagiellonian University, Ingardena 3, 30-060, Kraków, Poland. E-mail: podgajny@chemia.uj.edu.pl*
[b]*H. Niewodniczański Institute of Nuclear Physics PAN, Radzikowskiego 152, 31-342, Kraków, Poland*
[c]*Department of Solid State Physics, Faculty of Physics and Applied Computer Science, AGH University of Science and Technology, Mickiewicza 30, 30-059, Kraków, Poland*

† Electronic supplementary information (ESI) available: detailed crystallographic data for **2** and **3** in the form of CIF and RES files; Table S1: The most important distances within Cu–N–C–W linkages in **2** and **3**; Fig. S1: The $k^2\cdot\chi(k)$ functions obtained from the W L_3 edge spectra of compounds **1** and **2**; Fig. S2: $M(H)$ curves for **2** and **3** at $T = 4.3$ K; Fig. S3: The illustration of the inflection point in $M(H)$ curves at $T = 4.3$ K and 18.6 K for **2**. See DOI: 10.1039/b703640j

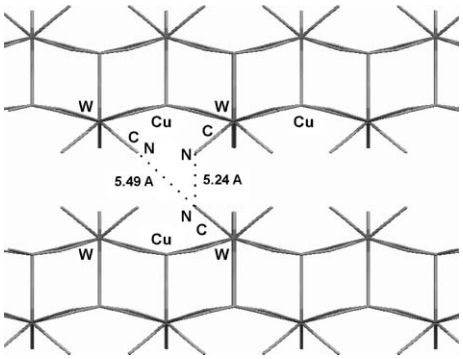

Scheme 1

metallic cation leading to the formation of a heterotrimetallic 3D coordination framework. This would modify the magnetic properties of the original bilayered $\{(LH_x)Cu^{II}_x[M^V(CN)_8]_x \cdot yH_2O\}_n$ system. Therefore, we performed the heterogeneous reaction between solid $(dienH_3)\{Cu^{II}[W^V(CN)_8]\}_3 \cdot 4H_2O$ (**1**) and an aqueous solution of $Dy^{III}(NO_3)_3$. The process did not lead to the expected trimetallic compound. Instead, the novel 3D cyano-bridged non-stoichiometric $Cu^{II}_{2.44}\{Cu^{II}_4[W^V(CN)_8]_{3.12}[W^{IV}(CN)_8]_{0.88}\} \cdot 5H_2O$ (**2**) was obtained. Here we present its crystal structure, spectroscopic characterisation and magnetic properties. We also compare its properties to structurally related $Cu^{II}_{2.97}\{Cu^{II}_4[W^V(CN)_8]_{2.06}[W^{IV}(CN)_8]_{1.94}\} \cdot 4H_2O$ (**3**) synthesised in the direct reaction between $[Cu^{II}(H_2O)_6]^{2+}$ and $[W^V(CN)_8]^{3-}$.

Experimental

Materials and syntheses of precursors

$Cs_3[W(CN)_8] \cdot 2H_2O$ was prepared by the literature method.[21] Liquid dien ligand and $Cu(NO_3)_2 \cdot 3H_2O$ were purchased from Aldrich and used without further purification. All manipulations and measurements were carried out under red light due to the photosensitivity of the octacyanotungstate(V) ions.[22,23] The precursor $(dienH_3)\{Cu^{II}[W^V(CN)_8]\}_3 \cdot 4H_2O$ **1** was obtained according to the optimised literature procedure.[20] Briefly, an acidic (pH $\sim$ 1.5, HNO_3) aqueous solution of $Cs_3[W^V(CN)_8] \cdot 2H_2O$ (5 mmol, 4.14 g, 75 ml) was slowly added to an acidic (pH $\sim$ 1.5, HNO_3) mixture of $[Cu^{II}(H_2O)_6](NO_3)_2$ (5 mmol, 1.21 g, 70 ml) and diethylenetriamine (6 mmol, 0.66 ml). After 10 minutes a green polycrystalline powder precipitated. The product was filtered under suction, washed with water and dried in air. Yield: 60%. Found: C, 21.85%; H, 1.41%; N, 24.46%. Calc. for $C_{28}H_{24}N_{27}Cu_3O_4W_3$: C, 21.77%; H, 1.57%; N, 24.48%. The identity of powder solid **1** was also confirmed by IR spectroscopy, X-ray powder diffraction and AC susceptibility measurements.

Synthesis of $Cu^{II}_{2.44}\{Cu^{II}_4[W^V(CN)_8]_{3.12}[W^{IV}(CN)_8]_{0.88}\} \cdot 5H_2O$ 2

The complete conversion of precursor **1** to product **2** was achieved *via* the following procedure: 0.5 g (0.32 mmol) of **1** was allowed to stand in a concentrated aqueous solution of $Dy(NO_3)_3$ (5.26 g, 1.2 mmol, 10 ml) for two weeks. The resulting grey-green solid **2** was filtered under suction, washed with distilled water and dried in air. Yield: 0.18 g, 20%. Found: C, 19.38%; H, 0.77%; N, 21.35%. Calc. for $C_{32}H_{10}Cu_{6.44}N_{32}O_5W_4$: C, 18.59%; H, 0.49%; N, 21.68%. The molar ratio of Cu : W was found to be very close to 3 : 2 using the Proton Induced X-ray Emission (PIXE) method. No traces of dysprosium in **2** were detected. IR spectrum, ν/cm^{-1}: 3600–3200vs(br), 2241m, 2202vs, 2163s, 1646s, 1613w(sh), 542w, 490s, 467w. Compound **2** was characterised structurally by X-ray powder diffraction and X-ray absorption spectroscopy. Similar **1** $\rightarrow$ **2** conversion was generally observed in a series of biphasic solid–liquid systems consisting of concentrated aqueous solutions of electrolytes: KNO_3, KNO_3–HNO_3 and $Fe(NO_3)_3$.

Synthesis of $Cu^{II}_{2.97}\{Cu^{II}_4[W^V(CN)_8]_{2.06}[W^{IV}(CN)_8]_{1.94}\} \cdot 4H_2O$ 3

The microcrystalline powder sample of compound **3** was obtained *via* a slow diffusion reaction between $[Cu^{II}(H_2O)_6](NO_3)_2$ and $Cs_3[W^V(CN)_8]$ in aqueous media in a H-tube. Yield: 100 mg, Found: C, 18.65%; H, 0.77%; N, 21.61%. Calc. for $C_{32}H_8Cu_{6.97}N_{32}O_4W_4$: C, 18.45%; H, 0.39%; N, 21.52%. IR spectrum, ν/cm^{-1}: 3600–3200vs(br), 2241m, 2202vs, 2163s, 1647s, 1612w(sh), 543w, 492s, 466w. Compound **3** was characterised structurally by powder X-ray diffraction.

X-Ray powder diffraction data collection and structure solution

X-Ray powder diffraction measurements for **1**, **2** and **3** were performed on a Philips X'Pert Pro diffractometer with a Bragg–Brentano geometry using CuKα radiation (λ = 1.54178 Å). The patterns were collected at 298 K between 5 and 60° 2θ angle.

The powder diffraction patterns were indexed using the PROSZKI package.[24] The best solutions give unit cells with parameters: for **1**: a = 7.391(1) Å, b = 32.277(5) Å, c = 7.029(1) Å, V = 1676.3(4) Å^3, F_{30} = 54.62,[25] space group $Cmc2_1$; for **2**: $a = b$ = 7.2704(4) Å, c = 28.261(3) Å, V = 1493.9(2) Å^3, F_{30} = 59.67; space group $I4/mmm$, for **3**: $a = b$ = 7.2732(9) Å, c = 28.236(5) Å, V = 1501.3(4) Å^3, F_{30} = 65, space group $I4/mmm$. The starting model for the refinement of the structure of **2** and **3** was built on the basis of single crystal data of $Cs_2Cu^{II}_7[Mo^{IV}(CN)_8]_4 \cdot 6H_2O$ (tetragonal system, space group $I4/mmm$, cell parameters: $a = b$ = 7.2444(9) Å, c = 28.417(5) Å, V = 1491.4(4) Å^3).[9] Rietveld refinement of the structures of **2** and **3** was carried out using the program JANA2000.[26] Initial profiles were obtained by fitting the observed pattern according to the LeBail method.[27] Refinement included scale, zero-point, background, preferred orientation, lattice parameters, atomic positions, occupancy and isotropic displacement. To account for the preferred orientation the March–Dollase function was used.[28] The atomic coordinates were refined using restraints d(W–C) = 2.15 ($\pm$5), d(Cu–N) = 2.00 ($\pm$5) and d(C–N) = 1.15 ($\pm$2), respectively. Interlayer atoms of C_{CN}, N_{CN}, and O were refined with fixed partial occupancy: cyanides C2N2 (0.75 occupancy) and water molecules (0.125 occupancy) for **2**, and cyanides C2N2 (0.375 occupancy) for **3**. Occupation of Cu2 atoms in both compounds was refined separately. The values of site occupancy factors obtained are 0.61(2) for **2** and 0.37(1) for **3**. The final agreement factors are R_p = 0.0251 and R_{wp} = 0.0249 for **2**; and R_p = 0.0525 and R_{wp} = 0.0436 for **3**.

Physical techniques

Infrared spectra were measured in KBr pellet form between 4000 and 400 cm^{-1} using a Bruker EQUINOX 55 spectrometer. X-Ray absorption measurements were carried out at the A1 beamline at Hasylab/DESY, Hamburg. Copper K edge and tungsten L_3 edge spectra were measured for the **1** and **2** powder samples at room temperature using a four crystal Si(111) monochromator. The energy resolution $\Delta E/E$ was estimated to be about 0.2×10^{-4} for all the measurements. The transmission mode and the total fluorescence yield detection mode was used. Measurements were also carried out on the samples of CuBr and $CuCl_2$ serving as references of Cu^{I} and Cu^{II} respectively. The magnetic measurements were carried out using a 7225 Lake Shore AC Susceptometer/DC Magnetometer. The thermal dependence of magnetic susceptibility was measured at a H_{dc} field of 1 kOe in the temperature range 4.2–240 K. The thermal dependences of the real χ' and imaginary χ'' AC magnetic susceptibility were measured in zero H_{dc} and oscillating magnetic field H_{AC} = 2 Oe. The field dependence of magnetisation was measured at 4.3 K in the 0–56 kOe magnetic field range.

Results and discussion

Crystal structures of 2 and 3

Fig. 1 compares the powder diffraction patterns of **1**, **2** and **3**. The index analysis indicates significant changes in the crystallographic cell parameters for the tetragonal unit in **2** ($a = b$ = 7.2695(9) Å, c = 28.268(5) Å, V = 1493.8(4) $Å^3$) and **3** ($a = b$ 7.2858(9) Å, c = 28.282(5) Å, V = 1501.3(4) $Å^3$) compared to the orthorhombic unit of **1** (a = 7.2732(9) Å, b = 32.277(5) Å Å, c = 7.029(1) Å, V = 1676.3(4) $Å^3$). The final Rietveld plots for **2** and **3** are shown in Fig. 2. Both assemblies contain Cu and W centres joined by cyano bridges (Fig. 3) giving the 3D cyano-bridged coordination network (Fig. 4). The Cu1 and W1 centres form the cyano-bridged $\{Cu[W(CN)_8]\}_n^{n-}$ double-layers perpendicular to the longest crystallographic period in a manner similar to assembly **1** (see Scheme 1). The metric parameters of the frameworks **2** and **3** did not change significantly compared to those of **1**.[20] Cu1 centres coordinate

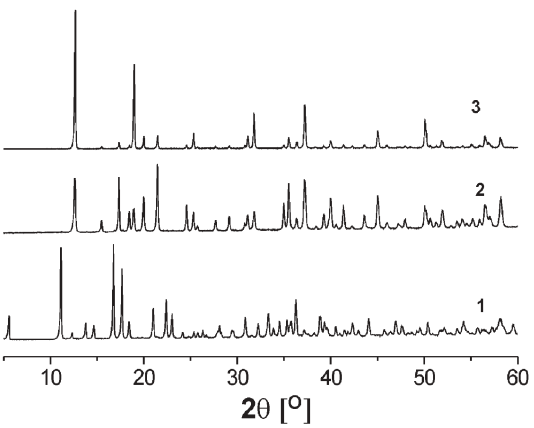

Fig. 1 Powder diffraction patterns of **1** (bottom), **2** (middle) and **3** (top).

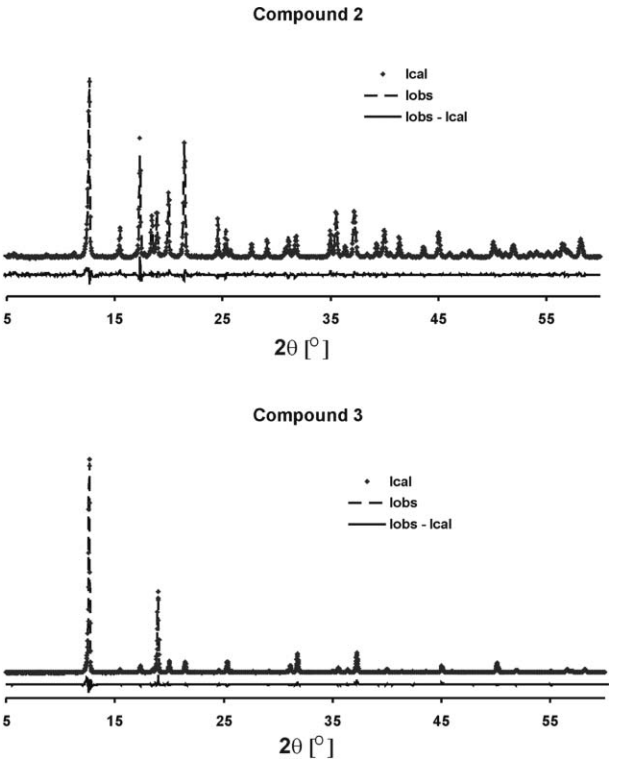

Fig. 2 Rietveld plots (crystal structure solution and refinement) for **2** (top) and **3** (bottom).

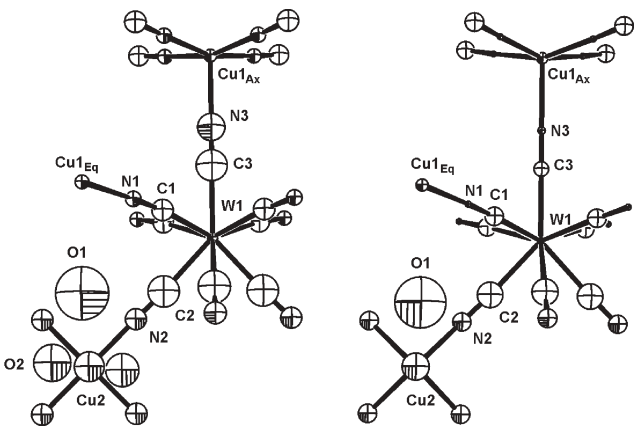

Fig. 3 Atom numbering scheme showing Cu–NC–W linkages in **2** (left) and **3** (right).

5 nitrogen atoms of $[W1(CN)_8]^{3-}$ moieties in square pyramidal geometry with equatorial Cu1–N1 distances of 1.957(12) (**2**) or 1.955 Å (**3**) and axial Cu1–N3 distances of 2.17(2) (**2**) or 2.18 Å (**3**). We observe also the O1 atoms being extremely weakly bonded to Cu1 centre with Cu1···O1 contact distances of 3.06 (**2**) and 3.26 Å (**3**). Cu2 centres of square planar geometry are located between the double-layers and coordinate four nitrogen atoms of CN^- ligands pointing out of the double-layers with Cu2–N2 distances of 1.955 (**2**) or 1.962 Å (**3**). The interlayer Cu2 centres together with their coordination spheres (N2, C2 and O2 atoms) reveal remarkable disorder implied by the starting model used for the refinement[9] (see Experimental). According to this model, five cyano bridges have full

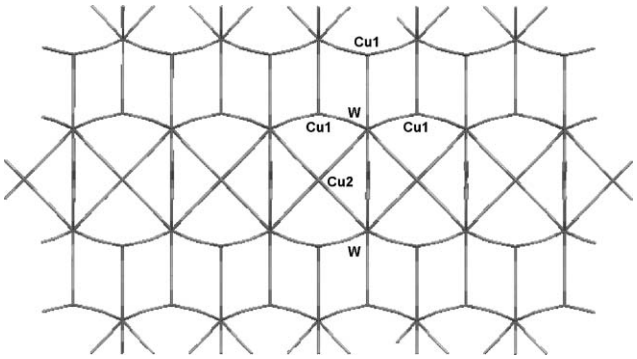

Fig. 4 Crystal packing diagrams **2** and **3** along the longest axes. O atoms are omitted for clarity.

occupancy 1.0 (four equatorial C1–N1 and one axial C3–N3 bridges between W1 and Cu1 for **2** and **3**). The three remaining cyano bridges (C2–N2 bridges between W1 and Cu2 for **2** and **3**) may be represented by 4 (**2**) or 8 (**3**) "bridges" positions with occupancies of 3/4 (**2**) and 3/8 (**3**), respectively. As a consequence, four (**2**) or eight (**3**) possible Cu2 crystallographic positions were obtained and their partial occupancies were refined separately (see Experimental). In the case of **2** additional O2 atoms of occupancy 0.125 were included for better refinement.

In both **2** and **3** W–C distances are within the range of 2.14–2.17 Å. The resulting W···Cu distances within W–C–N–Cu linkages are of 5.2–5.5 Å (ESI† Table S1 and Fig. 3). The closest W···W distances between $\{Cu[W(CN)_8]\}_n^{n-}$ bilayers are of 7.5 Å and are significantly shorter than the interlayer W···W distances of 9.7 Å in **1**. The calculated metric parameters for **2** and **3** confirm their similarity to the model compound $Cs_2Cu^{II}_7[Mo^{IV}(CN)_8]_4{\cdot}6H_2O$.[9]

The major difference between **2** and **3** consists of the number of copper centres located in the Cu2 crystallographic sites per $\{Cu[W(CN)_8]\}_4^{4-}$ bilayer unit. The non-stoichiometric number of Cu2 centres per formula unit exceeds 2 in both cases, being 2.44 for **2** and 2.97 for **3**. The excess of Cu(II) is compensated by the appropriate number of reduced octacyanotungstate(IV) moieties, 0.88 for **2** and 1.94 for **3**. This is consistent with IR spectroscopy and magnetic data (*vide infra*). The coexistence of $[W^V(CN)_8]^{3-}/[W^{IV}(CN)_8]^{4-}$ moieties was recently established for some cyano-bridged copper-octacyanotungstate compounds.[10,16]

IR spectroscopy

The IR spectra of **2** and **3** in the ν(CN) region exhibit 2241m, 2202s and 2163s cm^{-1} bands. This can be compared to the ν(CN) pattern of **1**, which exhibits 2203s and 2161m cm^{-1} bands. We attribute the band at 2241 cm^{-1} to cyano-bridging of increased rigidity (kinematic effect) of the W(V)–CN–Cu(II) linkage in **2** and **3**.[1] The broad 2163 cm^{-1} band of significantly increased intensity compared to **1** is predominantly assigned to the vibration of bridging CN ligands of the $[W^{IV}(CN)_8]^{4-}$ moiety, based on results obtained for cyano-bridged $W^{IV}Cu^{II}$ networks.[1,9,16,17] In the case of **2** no spectral features assignable to the C–C, N–C, N–H and C–H vibrations of organic molecules in the 1800-400 cm^{-1} region can be observed. This indicates practically complete removal of $dienH_3^{3+}$ cations on going from the original network **1** to **2**. In the region of γ(OH) vibrations of H_2O molecules two modes, 1646s and 1613w(sh) cm^{-1}, are seen. In the region of skeletal Cu–N and W–C vibrations three peaks located at 542w, 490s and 467 w cm^{-1} dominate. The 542 and 467 cm^{-1} bands are not seen in the spectrum of **1**. We attribute their presence to the additional Cu2–N2–C2–W1 linkages that appear in the cyano-bridged framework in **2** and **3**.[18]

X-Ray absorption spectroscopy (XAS) studies

The spectra in the Cu K-edge XANES range for **1** and **2** as well as for the reference samples of CuBr and $CuCl_2$ obtained in the transmission mode are presented in Fig. 5 (top). The edges for both samples studied have energies very similar to that of $CuCl_2$. This confirms that copper is in the valence state 2+ in both compounds.

The X-ray absorption spectra in the EXAFS range obtained in the total fluorescence yield detection mode were elaborated using the ATHENA[29] software. The EXAFS functions $\chi(k)$ were obtained from the experimental spectra by subtraction of the atomic absorption background, approximated by a spline function with the Rbk parameter of 0.9 Å for Cu K edge and 1.1 Å for the W L_3 edge. The $k^2{\cdot}\chi(k)$ functions for **1** and **2** are presented in Fig. 5 (middle) for copper and in ESI† Fig. S1 for tungsten. They were Fourier transformed using the Hanning window in the range of k = 2–8 $Å^{-1}$ taking into account the phase shift.

The EXAFS functions $\chi(R)$ of the two compounds obtained from the Cu K edge are presented in Fig. 5 (bottom). They exhibit two dominant peaks at about 2 Å and 3 Å of comparable intensities, which correspond to the next neighbour nitrogen and carbon atoms. They show no significant difference in their distances from the central Cu ion between the two compounds. Slightly smaller widths of the peaks for **2** are observed only, which indicates possibly a slightly narrower distribution of the neighbours within the 1st and 2nd coordination shells. The intensities of the two peaks are very similar in both compounds, which reflects a very similar coordination number of CN groups. A weak peak at about 5 Å corresponds to the transition metal (tungsten) neighbours. The EXAFS functions $\chi(R)$ of **1** and **2** obtained from the W L_3 edge spectra exhibit two strong peaks close to 2 Å and 3 Å, corresponding to carbon and nitrogen atoms, respectively. A weak peak located slightly above 5 Å is attributed to the Cu ions. Its larger intensity for **2** indicates the presence of an increased number of W–CN–Cu linkages compared to **1** (Fig. 6).

Magnetic properties

The $\chi T(T)$ dependences for **2** and **3** measured at H_{DC} 1 kOe are presented in Fig. 7. Both signals increase very slowly on cooling down to about 50 K, then increase more abruptly reaching the maxima of 625 (**2**) and 581 $cm^3\ mol^{-1}$ K (**3**) at 33 K. On cooling below this point, both signals decrease to about 20 (**2**) and 100 (**3**) $cm^3\ mol^{-1}$ K at 4.2 K with significant divergence of the $\chi T(T)$ curves. The important aspect is that the $\chi T(T)$ curve of **3** runs above that of **2** below 30 K. The best

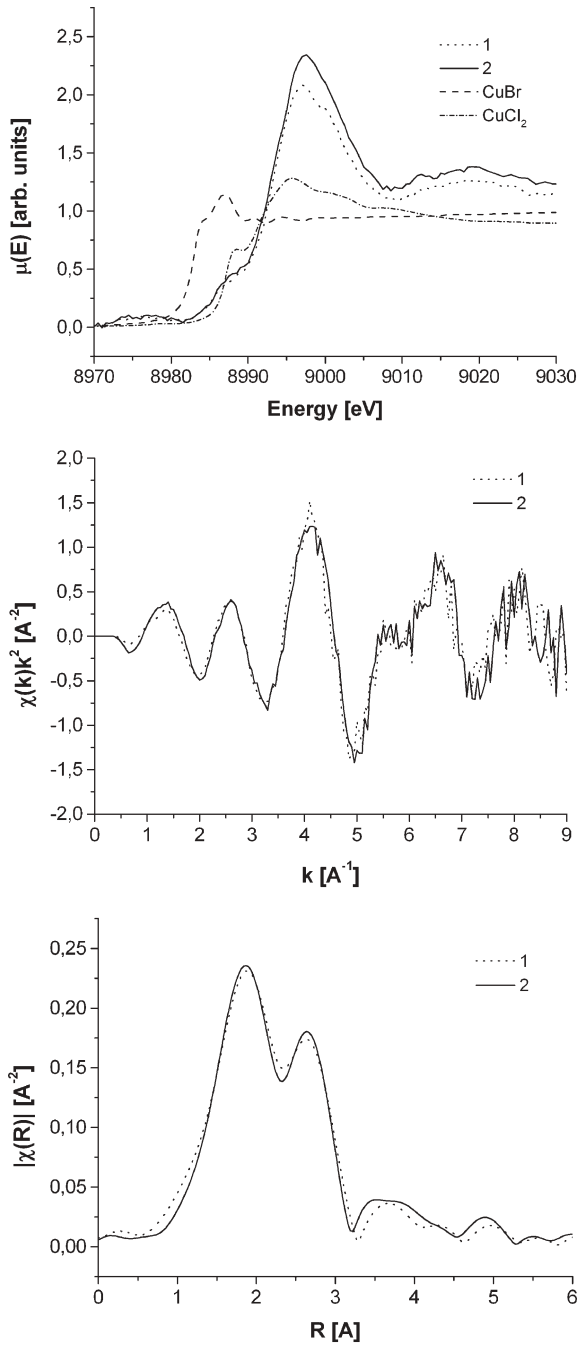

Fig. 5 X-Ray absorption spectroscopy of **1** and **2**: the XANES Cu K edge spectra together with those of reference samples CuBr and $CuCl_2$ (top); the $k^2 \cdot \chi(k)$ functions obtained from the Cu K edge spectra (middle); the Fourier transforms $\chi(R)$ of the EXAFS functions obtained from the Cu K edge spectra (bottom).

fit to the Curie–Weiss law was obtained in the 75–240 K temperature range with the Weiss constants $\theta = 49 \pm 3$ (**2**) and 50 ± 2 (**3**) K, pointing to the presence of long range ferromagnetic ordering. The values of the Curie constant $C = 4.6 \pm 0.6$ (**2**) and 4.5 ± 0.6 (**3**) $cm^3\ mol^{-1}$ K are in agreement with 4.1 (**2**) and 3.9 (**3**) $cm^3\ mol^{-1}$ K expected per formula unit assuming the isotropic $g = 2.0$ for W(V) and $g = 2.2$ for Cu(II).

The AC magnetic susceptibilities of **1**, **2** and **3** are presented in Fig. 8. **2** and **3** are characterised by the transition to the

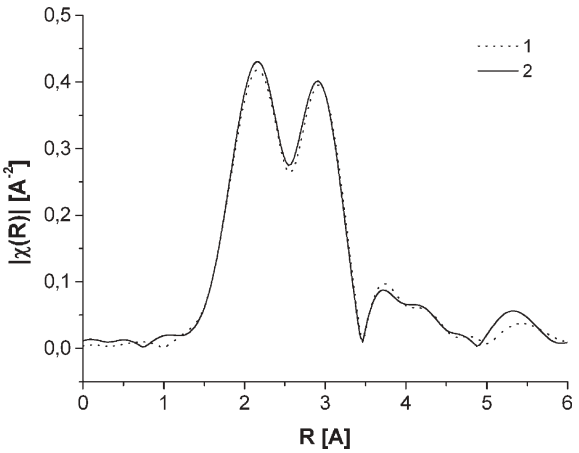

Fig. 6 The Fourier transforms $\chi(R)$ of the EXAFS functions obtained from the W L_3 edge spectra of compounds **1** and **2**.

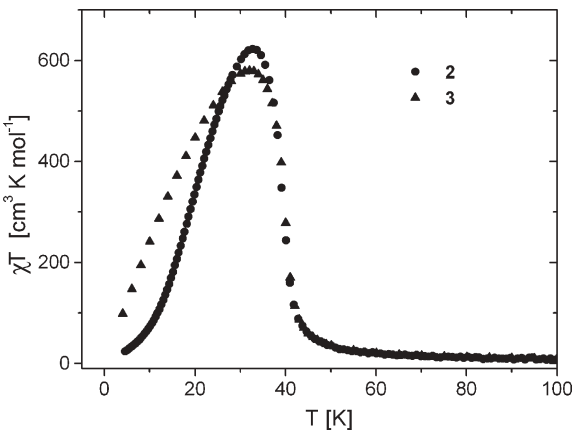

Fig. 7 The $\chi T(T)$ for **2** (circles) and **3** (triangles) (H_{DC} = 1 kOe).

ferromagnetically ordered phase at $T_C = 40$ K represented by a strong peak in the $\chi'(T)$ curves. The AC frequency independent χ' signal is accompanied by the out-of-phase χ'' component with the maximum appearing just below the maximum of χ'. The T_C value of 40 K in **2** and **3** is noticeably higher than 33 K found for **1** and manifests the enhanced magnetic coupling on altering of the 2D cyano-bridged skeleton of **1** into the 3D frameworks of **2** and **3**. The additional feature of $\chi'(T)$ curves for **2** and **3** is the presence of the second, less intense peak located slightly above 30 K. The area under the secondary peak is about 1.5% (**2**) and less than 1% (**3**) of the area under the main maximum at 40 K. Such a χ_{AC} singularity may appear at a spin reorientation transition or the magnetic domain rearrangement in the samples. In the case of **2**, the other reason may be a small admixture of an additional phase, the T_C of which is close to the T_C of **1**.

The low temperature magnetisation measurements reveal the values of magnetisation of saturation close to 9.11 (**2**) and 8.85 Nβ (**3**) at 56 kOe slowly approaching the high field limits of 9.56 Nβ (**2**) and 9.03 Nβ (**3**), respectively, expected for the formula units with a g_{iso} value of 2.00 (ESI† Fig. S2). The cyclic measurements of the $M(H)$ dependence at 4.3 K illustrate magnetic hysteresis loops with the values of coercive field H_c of 2 kOe for **2** and 2.5 kOe for **3** and remnant

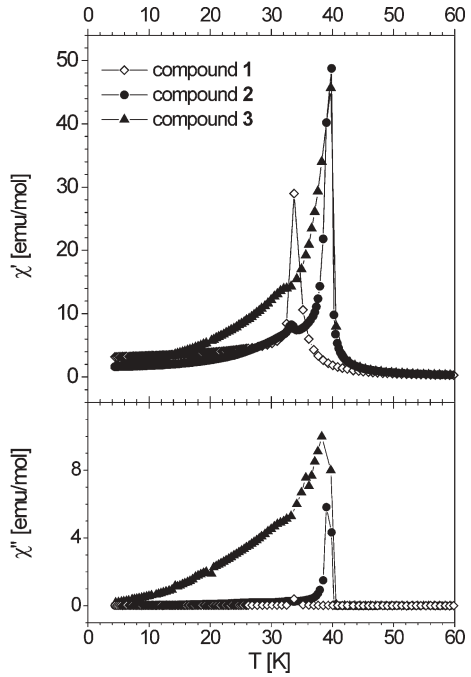

Fig. 8 The comparison of $\chi'(T)$ and $\chi''(T)$ for **1** (diamonds), **2** (circles) and **3** (triangles) (H_{AC} = 2 Oe).

magnetisation close to 4.5 Nβ (Fig. 9). The hysteresis loops are characterised by a magnetization jump (more pronounced for **2**) at the change of applied magnetic field direction with distinguishable steps at 0.5 kOe and −0.5 kOe. A marked $M(H)$ decrease at H = 0 may appear as a consequence of the presence of a soft magnetic phase in minute amounts. For **2**, a very small amount of easily magnetizing phase **1** may be present.[20]

Remarkably, the first cycle $M(H)$ curves in the magnetic field range 0–10 kOe are remarkably divergent (Fig. 9). For **2** the $M(H)$ dependence increases very slowly up to 0.8 kOe magnetization and only above this threshold field is the increase of the signal more rapid, with the $M(H)$ curve inflection point at 1.8 kOe. The threshold field decreases with temperature and at T = 18.6 K is 0.4 kOe (ESI† Fig. S3). Such

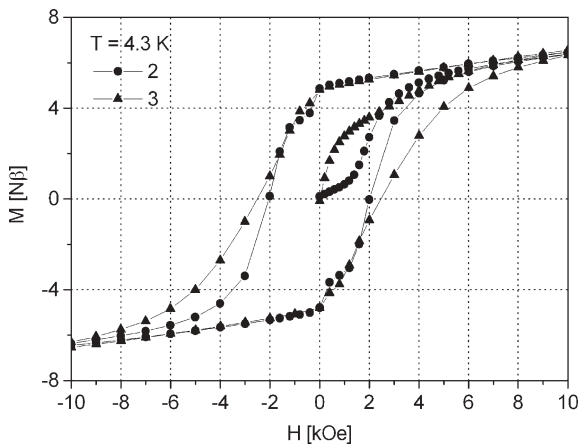

Fig. 9 Comparison of the magnetic hysteresis loops for **2** (circles) and **3** (triangles) at 4.3 K.

behaviour clearly indicates the metamagnetic character of network **2**. The relevant part of the $M(H)$ dependence of **3** shows an immediate fast increase of the signal, typical for 3D ferromagnets, converging with the $M(H)$ signal for **2** at about 6 kOe. This is in agreement with the course of $\chi T(T)$ dependences below T_{max} (Fig. 7). The appearance of these two types of long range magnetic ordering may be attributed to dissimilarities in the constitution of networks **2** and **3** per Cu_4W_4 bilayer unit: (i) different number of Cu2 atoms, 2.44 for **2**, and 2.97 for **3**, and (ii) occurrence of an adequate number of diamagnetic $[W(CN)_8]^{4-}$ moieties, 0.88 for **2** and, 1.94 for **3**. The presence of $[W(CN)_8]^{4-}$ non-magnetic "defects" is affecting magnetic dimensionality. The relatively low number of W(IV) centres in **2** permits the domination of the quasi-2D magnetic character like in **1** and in the related 2D coordination network with L = tetren (see Introduction, Scheme 1). For the latter, strong easy plane anisotropy has been estimated from the single crystal heat capacity data,[30] while for both compounds the deviation from the isotropic behaviour was observed by means of the χ_{AC} critical scaling.[5] Much higher number of W(IV) "defects" in **3** attenuates the 2D character of the ordering in favour of 3D character with comparable interactions through Cu1–W1 and Cu2–W1 pathways. Despite the expected different magnetic anisotropy, the same T_C value for **2** and **3** points to equal net exchange interactions. This is consistent with the strongest ferromagnetic coupling, inherent in all systems under study, as a result of CN-bridged interaction of unpaired $Cu^{II}(3d_{x^2-y^2})$ and $W^{V}(5d_{z^2}; 5d_{x^2-y^2})$ electrons residing at the orthogonal orbitals of the Cu1(II)–W(V) pair perpendicular to the bilayer.

The difference in the magnetic anisotropy presumed above for **2** and **3** is reflected in the temperature dependences of χ_{AC}. In general, the magnetic susceptibility below T_C at low fields is proportional to the square of the saturation magnetization and inversely proportional to the anisotropy constant, $\chi_{AC}(T) \propto M_s^2(T)/K(T)$.[31] Taking $M_s(T)$ equal for **2** and **3** results in higher χ_{AC} values for the more isotropic compound **3**.

We note that the magnetic properties of **2** and **3** resemble the ferromagnetic properties of $Cu_3[W(CN)_8]_2 \cdot 8H_2O$ material with T_C at 40 K reported earlier without structural characterisation and without detailed interpretation of the magnetic data.[32]

Conclusions

The self assembly of Cu(II) and $[W(CN)_8]^{3-}$ building blocks results in novel non-stoichiometric $Cu^{II}_{2+x}\{Cu^{II}_4[W^{V}(CN)_8]_{4-2x}[W^{IV}(CN)_8]_{2x}\} \cdot yH_2O$ 3D coordination networks with constitution dependent on the synthetic strategy. The alteration of dimensionality of cyano-bridged Cu(II)–W(V) framework from 2D to 3D leads to the increase of T_C, the ferromagnetic ordering temperature, from 33 K to 40 K and the increase of hardness represented by the value of the coercive field of 0.2 kOe (**1**), 2.0 (**2**) and 2.5 kOe (**3**). The subtle dissimilarities in the constitutions of **2** and **3**, related to different numbers of Cu2 atoms (2.44 for **2**, and 2.97 for **3**) and the occurrence of an adequate number of diamagnetic $[W(CN)_8]^{4-}$ moieties (0.88 for **2** and 1.94 for **3**) per Cu_4W_4 bilayer unit, affect the magnetic anisotropy and

dimensionality. The assembly **2** exhibits metamagnetic behaviour, while compound **3** resembles a classical 3D ferromagnet.

Acknowledgements

This research is partially supported by the Committee for Scientific Research of Poland (KBN) grant 3T09A 15 126 and NoE "MAGMANet" (NMP3-CT-2005-515767). Thanks are due to Dr Janusz Wolny for performing the PIXE measurements.

References

1 Sh. Ohkoshi, N. Machida, Zh. J. Zhong and K. Hashimoto, *Synth. Met.*, 2001, **122**, 523.
2 S. Ohkoshi, Y. Arimoto, T. Hozumi, H. Seino, Y. Mizobe and K. Hashimoto, *Chem. Commun.*, 2003, 2772.
3 R. Podgajny, T. Korzeniak, M. Bałanda, T. Wasiutyński, W. Errington, T. J. Kemp, N. W. Alcock and B. Sieklucka, *Chem. Commun.*, 2002, 1138.
4 D. Li, L. Zheng, X. Wang, J. Huang, S. Gao and W. Tang, *Chem. Mater.*, 2003, **15**, 2094.
5 M. Bałanda, T. Korzeniak, R. Pełka, R. Podgajny, M. Rams, B. Sieklucka and T. Wasiutyński, *Solid State Sci.*, 2005, **7**, 1113.
6 G. Rombaut, M. Verelst, S. Golhen, L. Ouahab, C. Mathonière and O. Kahn, *Inorg. Chem.*, 2001, **40**, 1151.
7 J. M. Herrerra, V. Marvaud, M. Verdaguer, J. Marrot, M. Kalisz and C. Mathoniere, *Angew. Chem., Int. Ed.*, 2004, **43**, 5468.
8 L. Catala, C. Mathonière, A. Gloter, O. Stephan, Th. Gacoin, J. P. Boilot and T. Mallah, *Chem. Commun.*, 2005, 746.
9 T. Hozumi, K. Hashimoto and Sh. Ohkoshi, *J. Am. Chem. Soc.*, 2005, **127**, 3864.
10 F. Chen, D. Li, S. Gao, X. Wang, Y. Li, L. Zheng and W. Tang, *Dalton Trans.*, 2003, 3283.
11 Y. S. You, J. H. Yoon, J. H. Lim, H. Ch. Kim and Ch. S. Hong, *Inorg. Chem.*, 2005, **44**, 7063.
12 T. Korzeniak, K. Stadnicka, M. Rams and B. Sieklucka, *Chem. Commun.*, 2005, 2939.
13 J. Larionova, R. Clérac, B. Donnadieu, St. Willemin and Ch. Guérin, *Cryst. Growth Des.*, 2003, **3**, 267.
14 D. Li, S. Gao, L. Zheng, W. Sun, T. Okamura, N. Ueyama and W. Tang, *New J. Chem.*, 2002, **26**, 485.
15 D. Li, S. Gao, L. Zheng, K. Yu and W. Tang, *New J. Chem.*, 2002, **26**, 1190.
16 R. Podgajny, T. Korzeniak, K. Stadnicka, Y. Dromzee, N. W. Alcock, W. Errington, K. Kruczała, M. Bałanda, T. J. Kemp, M. Verdaguer and B. Sieklucka, *Dalton Trans.*, 2003, 3458 and references therein.
17 Zh. X. Wang, P. Zhang, X. F. Shen, Y. Song, X. Z. You and K. Hashimoto, *Cryst. Growth Des.*, 2006, **6**, 2457.
18 T. Korzeniak, K. Stadnicka, M. Rams and B. Sieklucka, *Inorg. Chem.*, 2004, **43**, 4811.
19 J. H. Lim, J. S. Kang, H. Ch. Kim, E. K. Koh and Ch. S. Hong, *Inorg. Chem.*, 2006, **45**, 7821.
20 T. Korzeniak, R. Podgajny, N. W. Alcock, K. Lewiński, M. Bałanda, T. Wasiutyński and B. Sieklucka, *Polyhedron*, 2003, **22**, 2183.
21 L. D. C. Bok, J. G. Leipoldt and S. S. Basson, *Z. Anorg. Allg. Chem.*, 1975, **415**, 81.
22 K. R. Butter, T. J. Kemp, B. Sieklucka and A. Samotus, *J. Chem. Soc., Dalton Trans.*, 1986, 1217.
23 B. Sieklucka and A. Samotus, *J. Photochem. Photobiol., A*, 1993, **74**, 115.
24 W. Łasocha and K. Lewiński, *J. Appl. Crystallogr.*, 1994, **27**, 437.
25 G. S. Smith and R. L. Snyder, *J. Appl. Crystallogr.*, 1979, **12**, 60.
26 V. Petricek, M. Dusek and L. Palatinus, *Jana 2000, The crystallographic computing system*, Institute of Physics, Praha, Czech Republic, 2000.
27 A. LeBail, H. Duroy and J. L. Fourquet, *Mater. Res. Bull.*, 1988, **23**, 447.
28 W. A. Dollase, *J. Appl. Crystallogr.*, 1986, **19**, 267.
29 B. Ravel and M. Newville, *J. Synchrotron Radiat.*, 2005, **12**, 537.
30 R. Pełka, M. Bałanda, T. Wasiutyński, Y. Nakazawa, M. Sorai, R. Podgajny and B. Sieklucka, *Czech. J. Phys.*, 2004, **54**, D595.
31 H. A. Groenendijk, A. J. van Duyneveldt and R. D. Willet, *Physica B*, 1980, **101**, 320.
32 Y. Song, Sh. Ohkoshi, H. Seino, Y. Mizobe and K. Hashimoto, Synthesis, Crystal Structure and Metamagnetic Behaviour for Glycine Containing Tungstate(V) Copper(II) Bimetallic Polycyanide, VIIIth International Conference on Molecule Based Magnets ICMM'2002, Valencia, Spain, 5–10 October 2002, poster A-73.

